J Comput Aided Mol Des (2013) 27:807–821
DOI 10.1007/s10822-013-9681-3

Ab initio study on the noncovalent adsorption of camptothecin anticancer drug onto graphene, defect modified graphene and graphene oxide

Nabanita Saikia · Ramesh C. Deka

Received: 4 July 2013 / Accepted: 3 October 2013 / Published online: 17 October 2013

Abstract The application of graphene and related nanomaterials like boron nitride (BN) nanosheets, BN-graphene hybrid nanomaterials, and graphene oxide (GO) for adsorption of anticancer chemotherapeutic camptothecin (CPT) along with the effect on electronic properties prior to functionalization and after functionalization has been reported using density functional theory (DFT) calculations. The inclusion of dispersion correction to DFT is instrumental in accounting for van der Waals π–π stacking between CPT and the nanomaterial. The adsorption of CPT exhibits significant strain within the nanosheets and noncovalent adsorption of CPT is thermodynamically favoured onto the nanosheets. In case of GO, surface incorporation of functional groups result in significant crumpling along the basal plane and the interaction is basically mediated by H-bonding rather than π–π stacking. Docking studies predict the plausible binding of CPT, CPT functionalized graphene and GO with topoisomerase I (top 1) signifying that CPT interacts through π stacking with AT and GC base pairs of DNA and in presence of nano support, DNA bases preferentially gets bound to the basal plane of graphene and GO rather than the edges. At a theoretical level of understanding, our studies point out the noncovalent interaction of CPT with graphene based nanomaterials and GO for loading and delivery of anticancer chemotherapeutic along with active binding to Top1 protein.

Keywords DFT · Camptothecin · Graphene · Molecular docking · Reactivity descriptors · Drug delivery

Introduction

The emergence of graphene since its discovery in 2004 [1] has projected tremendous research interest and is foreseen as a significant milestone in terms of outstanding ballistic transport [2], long mean free path at room temperature [3] integral and half integral quantum hall effect [4, 5] and massless relativistic carriers [6]. Research targeted towards understanding and exploiting the extraordinary physical and chemical properties of graphene based nanomaterials have led to the quest in its application for biomedical research and diagnostics like gene delivery [7, 8], cellular imaging [9], and tumour therapy [10]. For exmaple adsorption of single-stranded DNA (ss-DNA) onto graphene helps it to quench electron donors and protect biomolecules from enzymatic cleavage, and also as a carrier module for therapeutic agents [11, 12]. The significant progress made in the field of graphene research motivated in extension of the study to new class of novel 2D nanomaterials like BN nanosheets as it has the same structural framework as graphene [13]. BN nanosheets proffers with added advantages compared to graphene in terms of stability up to a temperature of 1,000 K, and resistant towards oxidation [14]. Unlike graphene, pristine BN sheets are either insulators or wide band gap semiconductors [15] which under usual conditions are not ideal for practical applications. Hence to overcome these traits, modification of the electronic properties of BN nanosheets by functionalization [16–18], and substitutional C-doping [19] are the commonly adopted methodologies to transform

Electronic supplementary material The online version of this article (doi:10.1007/s10822-013-9681-3) contains supplementary material, which is available to authorized users.

N. Saikia · R. C. Deka (✉)
Department of Chemical Sciences, Tezpur University, Napaam, Tezpur 784028, Assam, India
e-mail: ramesh@tezu.ernet.in

the electronic properties from an insulator to conductor. Presently, a number of approaches have been proposed to modulate the electronic properties of BN nanosheets, such as C adatom adsorption [20], defect introduction [21], fluorination [22], hydrogenation [23] and noncovalent functionalization with organic molecules [24]. Compared to defect free graphene, heteroatom doping and chemical modification of surface and edge states can tune (open up) the band gap of graphene at the Fermi level [25, 26]. In this regard, B and N atoms are the preferred choice for dopant atoms as the elements B and N bracket the element C in the periodic table and because of the similarity in atomic sizes, B and N atoms can induce hole/electron donor or acceptor states within the Fermi level of graphene [27]. A recent study by Manna and Pati onto $B_xN_yC_z$ co-doping onto graphene and BN sheets have shown that hexagonal shaped domain segregation of B_xN_y and C_z onto graphene and BN nanosheets are the most stable structures from energetics perspective compared to smaller domain [28]. The ab initio studies on the non-covalent adsorption of biologically important molecules on either planar or curved graphene and BN surfaces have been widely explored in literature [29–32].

The intervention of graphene in cancer chemotherapy: With the tremendous wide scale applications of CNTs in cancer therapy [33] investigating the pharmacological and toxicity profiles, graphene and GO have proffered with new opportunities pertaining to the biomedical applications. Regarding the intrinsic toxicity of graphene and GO, Liu et al. [34] showed that poly ethylene glycol (PEG) functionalized GO exhibit negligible in vitro toxicity even upon subjecting to a high concentration of 100 μg/mL. Their study showed that radio labelled PEGylated GO basically remains localized in reticuloendothelial system (RES) including liver and spleen. Contrary to their report, Wang et al. [35] studied the biocompatibility aspects of pristine GO on human fibroplast cells and mice and showed that >50 μg/mL of GO can exhibit chronic toxicity and lung granulomas formation. Fan and co-workers in a very recent study examined the distribution and biocompatibility of GO in mice using radiotracer technique and biological assays and observed GO to gets deposited within the lungs. GO exhibits long blood circulation time (half life of 5.3 ± 1.2 h) and low uptake in RES [36]. Of the wide range of anticancer drugs being widely used today CPT holds potential application [37], as it specifically inhibit DNA topoisomerase I (Top 1), which plays a major role in the process of DNA transcription (essential for cell replication) by relaxing the torsional stress induced by duplex DNA [38, 39]. DNA Top1 is an enzyme essential for relaxation of DNA during a number of critical cellular processes, including replication, transcription, and repair [40]. CPT which is a fluorescent compound is a potent inhibitor of leukemia cells abnormal growth [41] and reversibly binds transient Top 1-DNA. Ha et al. [42] assessed the toxic side effect of CPT against cervical and uterine tumour cell line SiHa with respect to mitochondrial mediated cell death process. CPT leads to cell apoptosis in SiHa cells by inducing mitochondrial membrane permeability changes leading to release of cytochrome C and activation of caspase-3.

Our study investigates the adsorption of CPT onto graphene, BN nanosheet, B_xN_y and C_z modified graphene and finally extending to GO sheets in a way to understand the energetics of CPT interaction onto graphene nanomaterial and its prototypes. Three different dimensions of the nanosheets are considered to investigate the effect of length of nanosheets on the adsorption profile of CPT. The noncovalent functionalization is further investigated using dispersion corrected DFT (DFT-D) which takes into consideration the weak π–π stacking interactions, and the results compared with DFT energetics. Finally molecular docking simulations are performed to investigate the probable binding mechanism of Top 1 with CPT drug along with CPT functionalized graphene and GO sheets. The focus of the paper is primarily to present a theoretical insight into the nature of interaction, and energetics of CPT interaction with graphene based nanomaterials and their likely potential application as drug delivery modules in anticancer chemotherapy.

Computational methodology

DFT

Three different dimensions of graphene sheet are considered namely, 5 ring (5 × 5), 6 ring (6 × 6), and 8 ring (8 × 8), respectively with the ends terminated by H-atoms to saturate the dangling bonds. Similar dimensions of B_xN_y and C_z doped graphene and BN nanosheet are considered to study the effect of doping on electronic properties of the nanosheets along with subsequent adsorption of CPT molecule. For 5 × 5 doped graphene and BN nanosheets, a six ring defect region is considered and with increase in the size of the nanosheet the domain sizes are varied. For the adsorption of CPT onto GO, an 8 × 8 GO sheet is considered as the model system is functionalized both at the surface and edge states. The initial distance between CPT and GO sheet is kept to 2.6 Å well within the noncovalent interacting distance. The structures of the nanosheets including CPT molecule are fully optimized at the generalized gradient approximation (GGA)–Perdew Burke Ernzerhof (PBE) level of calculation as implemented in $DMol^3$ program [43]. The double numerical basis set with polarization functional (DNP) is used for the calculations.

The SCF tolerance is taken to be 10^{-6} eV atom^{-1} and for plotting the volumetric properties like the frontier orbitals fine grid (0.15 Å grid intervals), and contour plots having isovalue of 0.03 au is chosen to produce a higher quality grid.

The adsorption energy of CPT on to the studied nanosheets and GO is calculated using the relation:

$$E_{\text{ads}} = E_{\text{CPT}} + E_{\text{NANOSHEET}} - E_{\text{NANOSHEET/CPT}} \quad (1)$$

where $E_{\text{NANOSHEET}}$ is the total energy of the nanosheet without CPT molecule, E_{CPT} is the total energy of CPT drug and $E_{\text{NANOSHEET/CPT}}$ the total energy of the combined system after full geometry optimization. The counterpoise correction was not necessary while calculating the adsorption energy (given by Eq. 1) using DMol^3 program as DMol^3 uses a numerical basis set that minimizes the basis set superposition error (BSSE).

In an N-electron system having total energy (E) and external potential υ ($\vec{r}$), the electronegativity (χ) is given by:

$$\chi = -\left(\frac{\delta E}{\delta N}\right)_{v(\vec{r})} = -\mu \quad (2)$$

where μ is defined as the negative of electronegativity. Physically, μ describes the escaping tendency of electrons from an equilibrium system. The greater the μ value, less stable or more reactive is the system and vice versa. The η is expressed in terms of second derivative of energy with respect to the external potential υ ($\vec{r}$) and is given by:

$$\eta = \frac{1}{2}\left(\frac{\delta^2 E}{\delta N^2}\right)_{v(\vec{r})} \quad (3)$$

According to Mulliken [44] the working equations for μ and η using the finite difference method are given by:

$$\mu = -\chi = -\frac{1}{2}(I + A) \quad (4)$$

and

$$\eta = \frac{1}{2}(I - A) \quad (5)$$

where I is the ionization potential and A the electron affinity of the molecule. The electrophilicity index defined by Parr [45] is given as:

$$\omega = \frac{\mu^2}{2\eta} \quad (6)$$

The electrophilicity index is a measure of electrophilicity of an electrophile; higher the electrophilicity of a molecule greater is its electrophilic character. It is a measure of the stabilization in energy after the system accepts electronic charge from the environment. For our study the emphasis is basically laid on the variation of η and μ values to compare the energetics of the studied systems.

Dispersion corrected DFT (DFT-D)

Hybrid DFT calculations which includes DFT-D correction are quite reasonable in describing the non-covalent interactions of CPT with graphene, defect modified graphene and BN sheets. Spin polarized DFT calculations are performed for non-periodic clusters using G09 program [46]. For describing the π-stacking interaction, optimized CPT, pristine and functionalized CPT/graphene, defect modified CPT/nanosheet and CPT/BN nanosheet systems are individually studied at the wB97XD/6–31G(d,p) level of calculations. The adsorption energies are calculated using Eq. (1) described above. Likewise, the HOMO–LUMO energy gap, and the dipole moments for the interactions have been studied and the results compared with DFT calculated values.

Molecular docking

Molecular docking is predominantly applied for computer aided drug designing as it aims in predicting the interaction between the receptor–ligand complexes which sometimes becomes difficult to study experimentally [47]. For docking simulation, the crystal structure of Top 1 enzyme was retrieved from protein data bank (PDB: 1T8I). The docking simulations are performed using Molegro Virtual Docker [48] for active binding of graphene functionalized CPT onto the protein, which proves an upper hand over the other available docking programs for its high accuracy, about 87 % [49]. The glided differential evolution algorithm combines the differential evolution optimization technique with a cavity prediction algorithm [50]. The docking score function is an extension of the piecewise linear potential (PLP) [51] which includes the H-bonding and electrostatic terms and re-rank scoring function identifies the most promising docking solution from the solutions obtained by the docking algorithm and further increases the docking accuracy. For each of the complexes we conducted 100 independent runs, each of the runs returning one solution (pose). The solutions are re-ranked and the highest ranked solution is taken as the best docked conformation with the protein. For CPT, the prediction of active site and drug binding site was done by performing the docking studies of CPT with Top 1. The best docked conformation was selected on the basis of MolDock score and re-ranks score values (all in arbitrary units) and visualized using Molegro Virtual Viewer and Chimera softwares. We performed docking simulations on CPT functionalized onto graphene, (considering that the docking trend will be same for all the other nanosheets) and GO nanosheets and the best re-rank

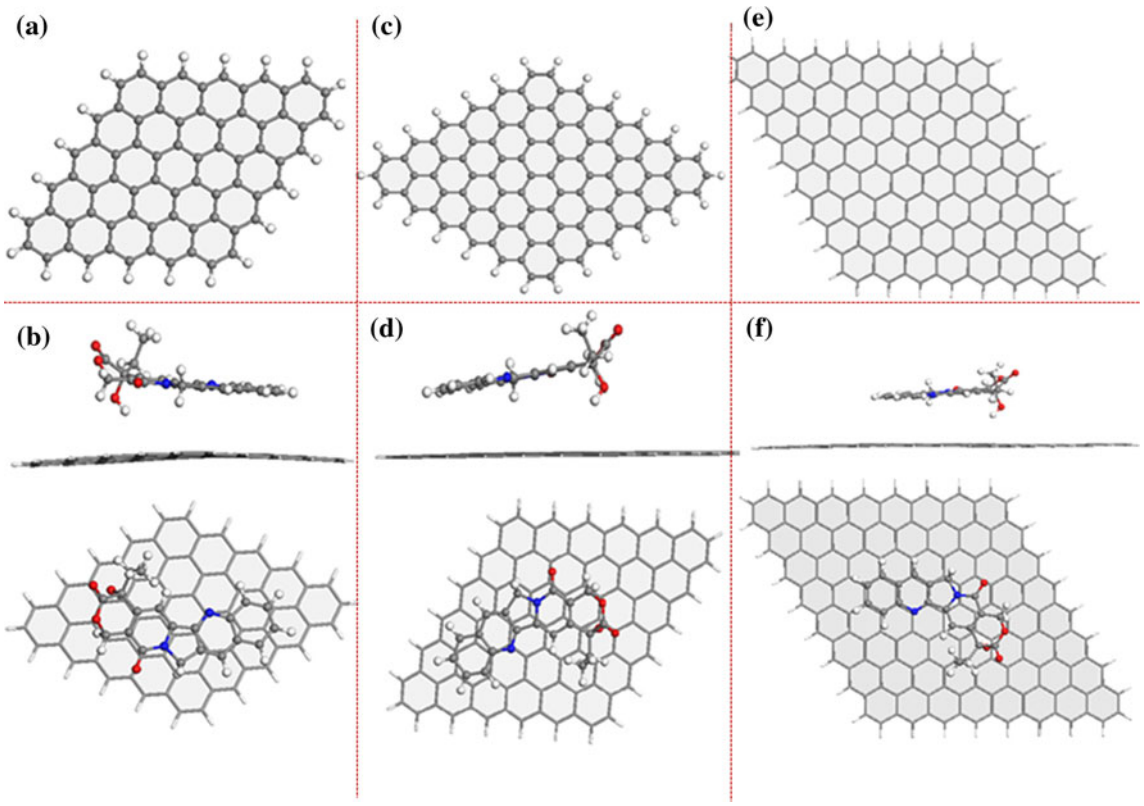

Fig. 1 The optimized geometries of **a** 5 × 5 graphene, **b** CPT adsorbed onto 5 × 5 graphene sheet depicting the side and front views, **c** 6 × 6 graphene, **d** CPT adsorbed onto 6 × 6 graphene sheet depicting the side and front views, **e** 8 × 8 graphene, **f** CPT adsorbed onto 8 × 8 graphene sheet depicting the side and front views

score value was chosen for further analysis. The 'simplex evolution', population size, maximum interactions, scaling factor, and crossover rate were set to 300, 150, 1000, 0.50, and 0.90, respectively.

Results and discussion

Structure and energetics

Figure 1 describes the optimized geometries of perfect and CPT functionalized 5 × 5, 6 × 6 and 8 × 8 graphene sheets. The average C–C bond length in graphene is calculated to be 1.42 Å. Upon functionalization, in CPT/5 × 5 graphene system slight deformations in graphene sheet is observed deviating from the planar conformation as opposed to perfect graphene. However, for 6 × 6 and 8 × 8 graphene sheets, the graphene surface assumes almost planar conformation as observed from Fig. 1d and f. In 6 × 6 graphene, CPT gets tilted with the aromatic ring getting inclined towards the graphene surface, which is not observed for the other graphene sheets indicating significant influence on the polarizability. The optimum interacting distances along with the adsorption energy values are provided in Table 1. Two factors basically govern the adsorption energies; one is the effective contact area between the CPT and graphene surface and the other is the atomic correlation between the aromatic rings of CPT and graphene surface. With the increase in dimension of graphene sheet, the adsorption energy value increases suggesting the thermodynamic favourability towards adsorption of CPT onto graphene surface and CPT undergoes stronger interaction with graphene sheet of higher dimension i.e. 8 × 8 graphene, and formation of such complexes is experimentally possible from energetics perspective. Another plausible explanation for the trend can be that adsorption of CPT onto small graphene sheet like 5 × 5 induces significant strain with the nanosheet proffering with low flexibility towards adsorption of CPT onto the surface compared to sheets of higher dimension. Except 8 × 8 graphene sheet where the aromatic ring of CPT sits perfectly on the hollow site, for 5 × 5 and 6 × 6 graphene sheets, CPT molecule prefers to be adsorbed at slipped hollow site. Although it is well known that DFT based GGA functional tend to underestimate the binding energy values for weak noncovalent interactions, the physical essence behind nature of interaction are not affected and we try to lay focus on this aspect.

Table 1 The adsorption energy (E_{ads}, eV), optimum distance of interaction, HOMO–LUMO energy gap and global reactivity descriptors for bare CPT, and CPT adsorbed onto graphene, BN nanosheet, BN and C doped graphene and BN nanosheets for the three studied dimensions of the sheet at the DMol^3 level of calculation

System	E_{ads}	Interacting distance	HOMO–LUMO gap	η	μ
CPT	–	–	2.288	1.144	−4.445
5 × 5 graphene	–	–	0.241	0.120	−3.907
CPT/5 × 5 graphene	0.222	3.779	0.242	0.121	−4.006
6 × 6 graphene	–	–	0.105	0.052	−3.939
CPT/6 × 6 graphene	0.822	3.761	0.126	0.063	−3.962
8 × 8 graphene	–	–	0.096	0.048	−3.938
CPT/8 × 8 graphene	1.245	3.741	0.099	0.049	−3.927
5 × 5 BN nanosheet	–	–	4.304	2.152	−3.509
CPT/5 × 5 BN nanosheet	0.547	4.117	2.273	1.136	−4.288
6 × 6 BN nanosheet	–	–	4.083	2.041	−3.528
CPT/6 × 6 BN nanosheet	1.038	3.956	2.295	1.147	−4.260
8 × 8 BN nanosheet	–	–	4.089	2.044	−3.470
CPT/8 × 8 BN nanosheet	1.302	3.943	2.253	1.126	−4.236
5 × 5 C-doped BN nanosheet	–	–	2.305	1.152	−3.532
CPT/5 × 5 C-doped BN nanosheet	0.541	3.881	1.873	0.936	−3.925
6 × 6 C-doped BN nanosheet	–	–	1.663	0.831	−3.541
CPT/6 × 6 C-doped BN nanosheet	1.067	3.954	1.623	0.811	−3.717
8 × 8 C-doped BN nanosheet	–	–	0.550	0.275	−3.533
CPT/8 × 8 C-doped BN nanosheet	1.486	3.945	0.543	0.271	−3.623
5 × 5 B_xN_y doped graphene	–	–	0.091	0.045	−3.858
CPT/5 × 5 B_xN_y doped graphene	1.028	4.319	0.101	0.050	−3.923
6 × 6 B_xN_y doped graphene	–	–	0.063	0.031	−3.892
CPT/6 × 6 B_xN_y doped graphene	1.123	3.935	0.078	0.039	−3.912
8 × 8 B_xN_y doped graphene	–		0.094	0.047	−3.953
CPT/8 × 8 B_xN_y doped graphene	1.419	3.916	0.096	0.048	−3.978
GO	–	–	0.084	0.042	−4.167
CPT/GO	1.324	4.109	0.088	0.044	−4.178

The optimized geometries of pure BN nanosheets (Fig. 2) depict an average B–N bond length of 1.457 Å. The optimized geometries suggest rumpling of BN nanosheets (Fig. 2b, d and f), with the BN sheet deviating from planar conformation and compared to CPT adsorption on graphene, the rippling observed for BN nanosheet is more prominent after adsorption. This shows that absorbed CPT molecule induces polarizability and prominent change in electronic properties of BN nanosheets, and the behaviour is almost independent of the sheet dimension. The optimum distance of interaction, adsorption energy values for CPT/BN nanosheet systems are provided in Table 1. Similar to the trend in variation of adsorption energy for CPT/graphene sheets, with increase in dimension of BN nanosheet, the adsorption energy value increases with 8 × 8 BN nanosheet exhibiting the highest value of adsorption energy of 1.302 eV at an optimum interacting distance of 3.943 Å. In all the three studied BN nanosheets, the aromatic ring of CPT sits perfectly at hollow site. The adsorption of CPT onto BN nanosheets is comparatively stronger than over graphene surface. The optimized geometries of pure C_z doped BN nanosheets are shown in Fig. 3. The average B–C, N–C and B–N bond lengths in the B_xN_y and C doped graphene and BN nanosheets are calculated to be 1.547, 1.406 and 1.469 Å, respectively. With increase in dimension of BN sheet, we varied the C_z domain segregated within the nanosheets as observed from Fig. 3a, c and e. Upon adsorption of CPT, significant crumpling of the doped nanosheet is observed with the CPT molecule getting adsorbed at hollow site for the three studied nanosheets. The adsorption energy value increases with increase in size of the nanosheet within the optimum interacting distance (Table 1) and follows the same trend as for perfect graphene and BN nanosheets, respectively. The adsorption of CPT onto 5 × 5 and 6 × 6 nanosheets retain their planar conformation whereas CPT adsorption onto 8 × 8 BN doped graphene

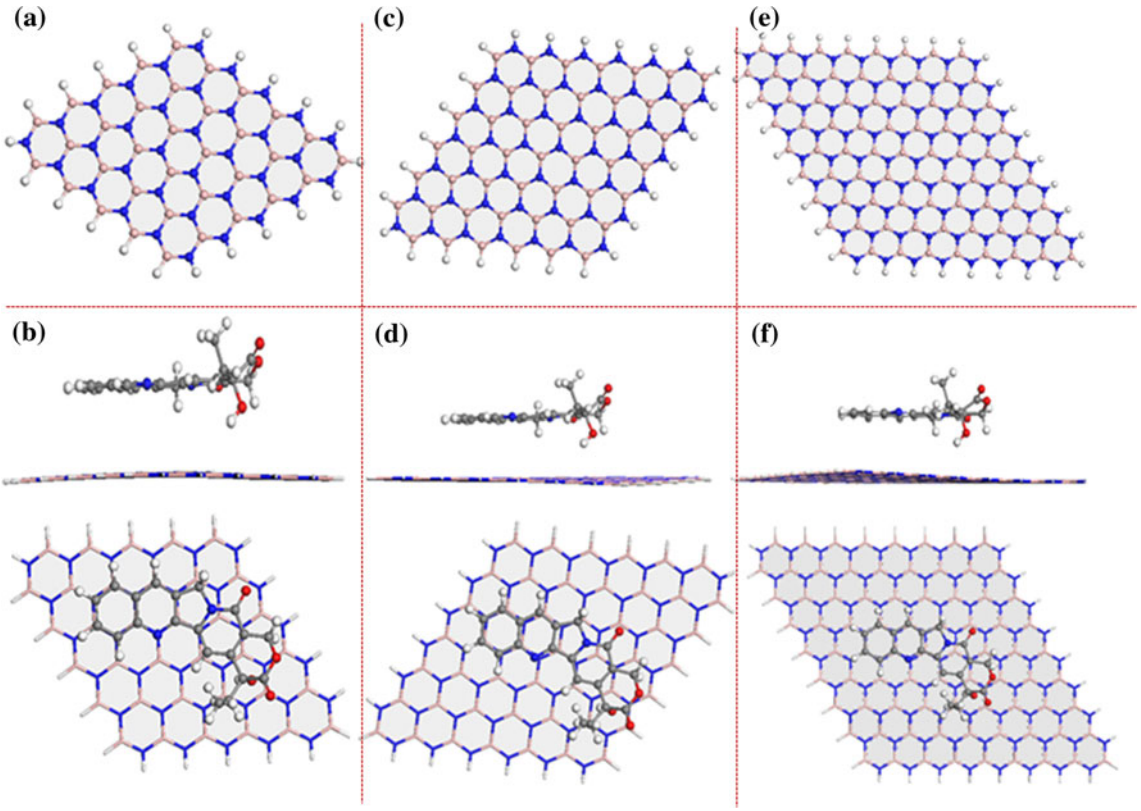

Fig. 2 The optimized geometries of **a** 5 × 5 BN sheet, **b** CPT adsorbed onto BN sheet depicting the side and front views, **c** 6 × 6 BN sheet, **d** CPT adsorbed onto 6 × 6 BN sheet depicting the side and front views, **e** 8 × 8 BN sheet, **f** CPT adsorbed onto 8 × 8 BN sheet depicting the side and front views

sheet shows the formation of a cusp in the doped region bearing the B_xN_y nanodomain (Fig. 4f). The optimum interaction distance and adsorption energy values follow a similar trend of increasing adsorption energy value with increase in size of the nanosheet. On an average, B_xN_y doped graphene exhibit higher adsorption energy values than C_z domain segregated BN nanosheets illustrating the fact that CPT has a higher thermodynamic preferentiality for adsorption onto BN nanosheets than over graphene. However, CPT adsorption onto B_xN_y and C_z doped 5 × 5 graphene and 5 × 5 BN nanosheets does not exhibit any rumpling of the sheet as observed from Figs. 3b and 4b.

Global reactivity descriptors

The CPT molecule is quite stable exhibiting a HOMO–LUMO gap of 2.288 eV and η value of 1.144 eV. A comparison of global reactivity descriptors for perfect and doped nanosheets without the adsorbed CPT molecule reveal BN nanosheet to be quite stable exhibiting an energy gap around 4.083–4.304 eV, the energy gap decreasing with increase in size of BN nanosheets. For B_xN_y and C doped graphene and BN nanosheets, BN doped graphene is quite reactive with lower energy gap of the order of 0.063–0.091 eV and η values of the order of 0.031–0.047 eV. C-doped BN nanosheets on the other hand, are comparatively less reactive than graphene but more reactive than BN nanosheets. The nanosheet with higher dimension favour stronger interaction with CPT molecule from a thermodynamic perspective. The variation of μ value do not follow any regular trend for the prefect and doped graphene and BN nanosheets. For graphene, BN nanosheet and C doped BN nanosheets the μ value decreases whereas for BN doped graphene the μ value increases with increase in the sheet dimension.

In case of graphene and BN doped graphene counterparts, adsorption of CPT shows a marked increase in stability of the nanosheets and η value illustrating that CPT adsorption renders stability to graphene and BN doped graphene systems. Adsorption of CPT onto perfect BN and C doped BN nanosheets demonstrate significant lowering in energy gap and η value reducing to almost half for BN nanosheet system which can be conducive with the comparatively higher E_{ads} values than that for perfect graphene system. Thus in general compared to adsorption of CPT onto graphene and BN doped graphene; BN nanosheet and C doped BN nanosheets exhibit quite demarked trend in the structural stability and reactivity of the nanosystems in turn

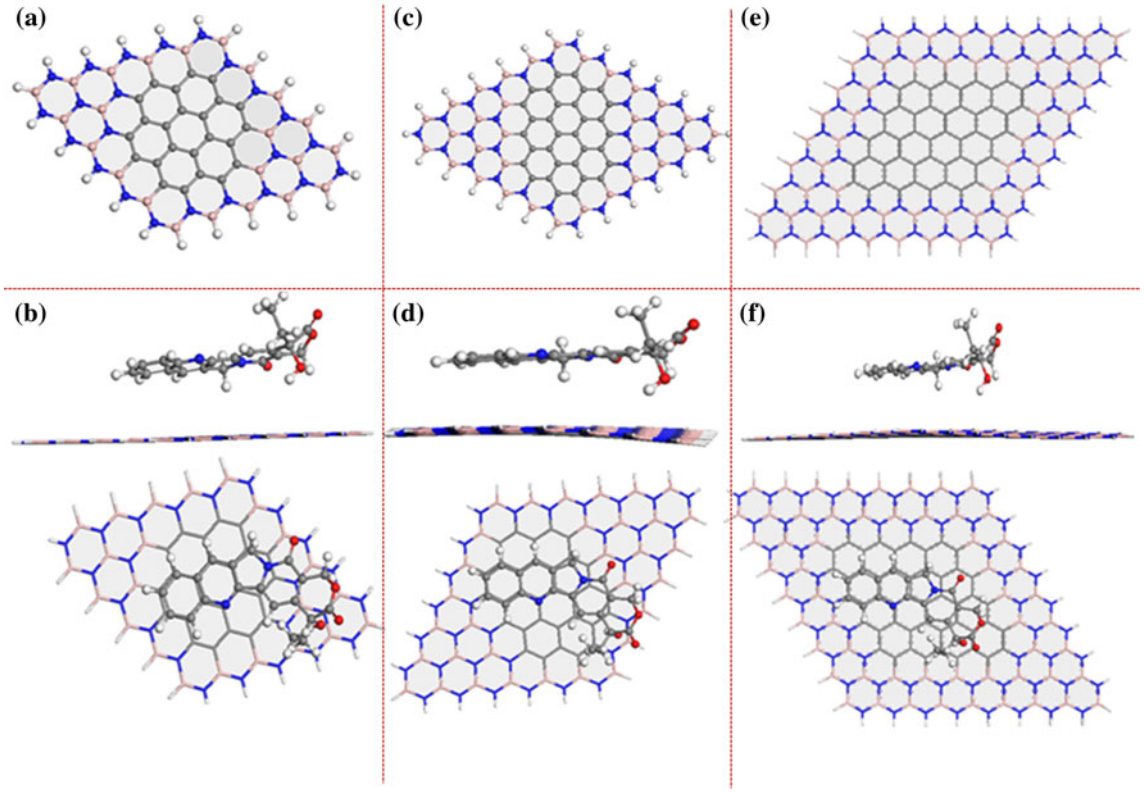

Fig. 3 The optimized geometries of **a** 5 × 5 C-doped BN sheet, **b** CPT adsorbed onto C-doped BN sheet depicting the side and front views, **c** 6 × 6 C-doped BN sheet, **d** CPT adsorbed onto 6 × 6 C-doped BN sheet depicting the side and front views, **e** 8 × 8 C-doped BN sheet, **f** CPT adsorbed onto 8 × 8 C-doped BN sheet depicting the side and front views

providing insight into the perturbation of electronic properties prior to and after functionalization. Secondly, presence of nanosystems for loading of CPT facilitates in the increased reactivity of CPT drug molecule compared to bare CPT drug.

Dispersion corrected DFT-D

Table 2 summarizes the adsorption energy, energy gap, global reactivity descriptors and dipole moment values for the studied systems. The variation of E_{ads} values within the same system as a function of the sheet dimension is quite in agreement to the trend in DFT with the adsorption energy value increasing with increase in sheet size. The DFT-D corrected adsorption energy values are comparatively higher than DFT-GGA calculated values and since realistic systems will result in higher adsorption interaction, DFT-D inclusion provide better correlation with the energetics of the system. Perfect BN and C-doped BN nanosheets exhibit maximum values of adsorption energy followed by B_xN_y doped graphene and perfect graphene systems. DFT-D correction illustrates the adsorption to be favoured onto doped nanosheet and perfect BN nanosheet systems as opposed to graphene from the thermodynamic perspective.

CPT adsorption onto graphene demonstrates an increase in HOMO–LUMO energy gap and η value suggesting an increase in stability of graphene/CPT system whereas for BN doped graphene except for 5 × 5 nanosheet, 6 × 6 and 8 × 8 nanosheets demonstrate a decrease in HOMO–LUMO and η values illustrating an increase in reactivity of the nanosystems. For BN nanosheet system, adsorption of CPT results in the increase in reactivity of CPT/BN nanosheets and follows the order: BN nanosheet > C doped BN nanosheet. The μ value on the other hand increases with increase in the dimension of the nanosheet and with functionalization of CPT onto the nanosheets suggesting an increase in reactivity of the system.

The dipole moment bears correlation with adsorption energy values; higher is the dipole moment greater is the extent of adsorption of CPT onto the nanosheets. Wu and co-workers [52] stated that the polarizability and lone pair of electron can affect the π–π stacking interaction. The dipole moment value is found to be highest for BN co-doped graphene sheet and follows the order:

BN doped graphene > C doped BN nanosheet > BN nanosheet > graphene (5 × 5 nanosheet)
C doped BN nanosheet > BN doped graphene > BN nanosheet > graphene (6 × 6 nanosheet)

Table 2 The adsorption energy (E_{ads}, eV), HOMO–LUMO energy gap, global reactivity descriptors and dipole moment values (Debye) for bare CPT, and CPT adsorbed onto graphene, BN nanosheet, BN and C doped graphene and BN nanosheets for the three studied dimensions of the sheet using GAUSSIAN09 program

System	E_{ads}	HOMO–LUMO gap	η	μ	Dipole moment
CPT	–	0.248	0.124	−0.167	10.282
5 × 5 graphene	–	0.065	0.032	−0.138	0.000
CPT/5 × 5 graphene	1.147	0.066	0.033	−0.142	6.341
6 × 6 graphene	–	0.041	0.021	−0.139	0.000
CPT/6 × 6 graphene	3.326	0.044	0.022	−0.141	6.275
8 × 8 graphene	–	0.033	0.017	−0.149	0.000
CPT/8 × 8 graphene	3.578	0.035	0.018	−0.150	7.299
5 × 5 BN nanosheet	–	0.370	0.185	−0.125	7.667
CPT/5 × 5 BN nanosheet	1.946	0.261	0.130	−0.155	8.193
6 × 6 BN nanosheet	–	0.361	0.180	−0.125	8.632
CPT/6 × 6 BN nanosheet	3.402	0.261	0.131	−0.156	9.256
8 × 8 BN nanosheet	–	0.353	0.176	−0.127	9.944
CPT/8 × 8 BN nanosheet	4.061	0.260	0.130	−0.156	11.358
5 × 5 C-doped BN nanosheet	–	0.238	0.119	−0.121	8.164
CPT/5 × 5 C-doped BN nanosheet	1.899	0.229	0.114	−0.133	9.266
6 × 6 C-doped BN nanosheet	–	0.197	0.098	−0.121	15.302
CPT/6 × 6 C-doped BN nanosheet	3.317	0.201	0.101	−0.128	21.289
8 × 8 C-doped BN nanosheet	–	0.062	0.031	−0.138	13.602
CPT/8 × 8 C-doped BN nanosheet	4.395	0.113	0.057	−0.126	20.379
5 × 5 B_xN_y doped graphene	–	0.048	0.024	−0.132	15.162
CPT/5 × 5 B_xN_y doped graphene	1.715	0.050	0.025	−0.135	17.097
6 × 6 B_xN_y doped graphene	–	0.079	0.040	−0.133	10.862
CPT/6 × 6 B_xN_y doped graphene	3.539	0.075	0.037	−0.134	12.385
8 × 8 B_xN_y doped graphene	–	0.062	0.031	−0.138	13.642
CPT/8 × 8 B_xN_y doped graphene	4.861	0.057	0.029	−0.138	20.268

BN doped graphene > C doped BN nanosheet > BN nanosheet > graphene (8 × 8 nanosheet)

Perfect graphene sheet exhibits zero dipole moment for the three studied dimensions and with functionalization the dipole moment value increases. Thus adsorption of CPT onto the nanosheets induces significant polarizability to the system in turn affect the charge transfer and conducting properties.

GO interaction with CPT: structure and energetics

Figure 5a and b depicts the optimized geometry corresponding to the front and side views of GO without the adsorbed CPT molecule. Due to the presence of surface functional groups the non-covalent interaction with CPT drug molecule will no more be governed by vdW interaction but rather mediated by H-bonding between the polar groups of CPT and GO at the close proximity of interaction. CPT adsorption onto GO is associated with an adsorption energy value of 1.324 eV. Compared to adsorption of CPT onto bare 8 × 8 graphene sheet associated with an adsorption value of 1.245 eV, GO favours the strong interaction between CPT (slipped hollow site of adsorption) mediated by the functional groups located on GO surface at the optimum interacting distance of 4.109 Å between the –OH group of CPT and GO basal plane. The optimized geometry of GO demonstrate significant crumpling of graphene basal plane and the induced curvature of GO due to the presence of covalently functionalized –OH and epoxy groups facilitate in the enhanced interaction of GO with CPT. A comparison of variation in HOMO–LUMO energy gap shows that GO is quite reactive than perfect graphene sheet exhibiting an energy gap of 0.084 eV quite obvious as covalent functionalization breaks the π delocalized network in graphene. Upon functionalization the energy gap increases to 0.088 eV suggesting that adsorbed CPT molecule induces stability to the otherwise reactive GO sheet. The trend observed for the variation of HOMO–LUMO gap and η value for GO is similar to that of perfect and BN co-doped graphene sheets (Table 1). The μ value on the other hand increases with

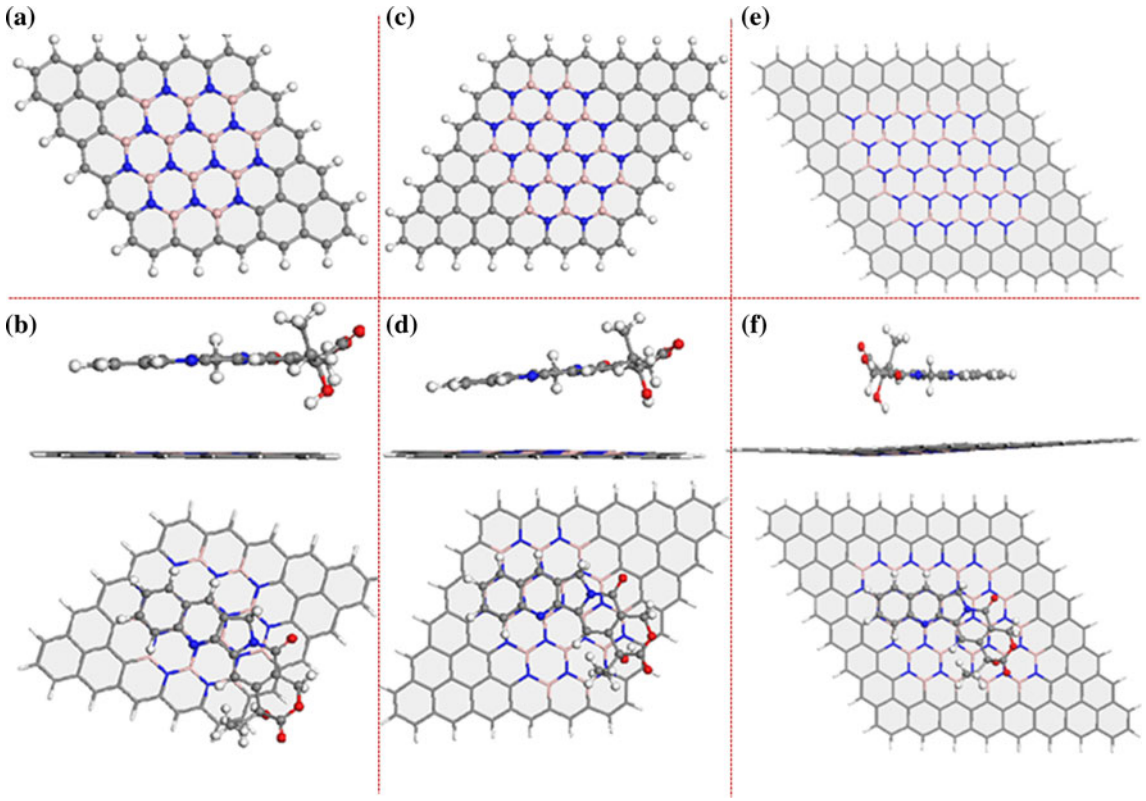

Fig. 4 The optimized geometries of **a** 5 × 5 BN-doped graphene, **b** CPT adsorbed onto 5 × 5 BN-doped graphene sheet depicting the side and front views, **c** 6 × 6 BN-doped graphene, **d** CPT adsorbed onto 6 × 6 BN-doped graphene sheet depicting the side and front views, **e** 8 × 8 BN-doped graphene, **f** CPT adsorbed onto 8 × 8 BN-doped graphene sheet depicting the side and front views

adsorption of CPT molecule indicating an increased tendency for charge transfer between GO and CPT molecule.

Frontier orbital analysis

The isosurface corresponding to HOMO of graphene (Fig. 6a, c, e) depict the electronic state to be localized along the edges with no contribution on the inner aromatic rings. Even with increase in dimension of graphene sheet, the trend in electronic states remains basically the same. The LUMO of graphene sheets (Supporting Information, Fig. S1a, c and e) also exhibit a similar trend as the HOMO. Upon functionalization, the trend in adsorption energy value remains mostly the same with contribution to the electronic state of HOMO (Fig. 6b, d and f) and LUMO (Supporting Information, Fig. S1b, d and f) isosurface coming from the graphene sheet and not from CPT molecule which shows that electronic state contribution towards the physisorption is essentially contributed from graphene rather than CPT molecule.

In case of perfect BN nanosheets, frontier orbital distribution corresponding to HOMO (Supporting Information, Fig. S2a, c and e) remains localized along one of the sheet edges with partial electron localization along the adjoining BN bonds and LUMO (Supporting Information, Fig. S3a, c and e) also remains localized along one of the BN edges along the terminal BH and NH bonds. For CPT adsorbed onto 5 × 5 and 6 × 6 BN nanosheets, HOMO (Supporting Information, Fig. 2b, d) and LUMO (Supporting Information, Fig. S3b and d) remains delocalized on the CPT molecule with no contribution on BN nanosheet, whereas for 8 × 8 nanosheet, the HOMO (Fig. S2f) is localized on BN sheet rather than CPT molecule and LUMO is delocalized over CPT molecule (Supporting Information, Fig. S3f).

On comparing the frontier orbital distribution for B_xN_y and C_z doped graphene and BN nanosheets, for C_z doped BN nanosheet, in absence of CPT, the HOMO (Supporting Information, Fig. S4a, c and e) remains delocalized along the C_z domain and adjoining B–C and N–C bonds with no contribution on BN rings of the nanosheet. As the size of BN domain increases as for 8 × 8 nanosheet, HOMO gets localized along the C domain with the delocalized electronic state of HOMO getting less uniform compared to 5 × 5 and 6 × 6 sheets. Upon adsorption of CPT, a similar trend in orbital distribution is noticed with HOMO remaining localized onto the C domains with no contribution on CPT molecule (Supporting Information,

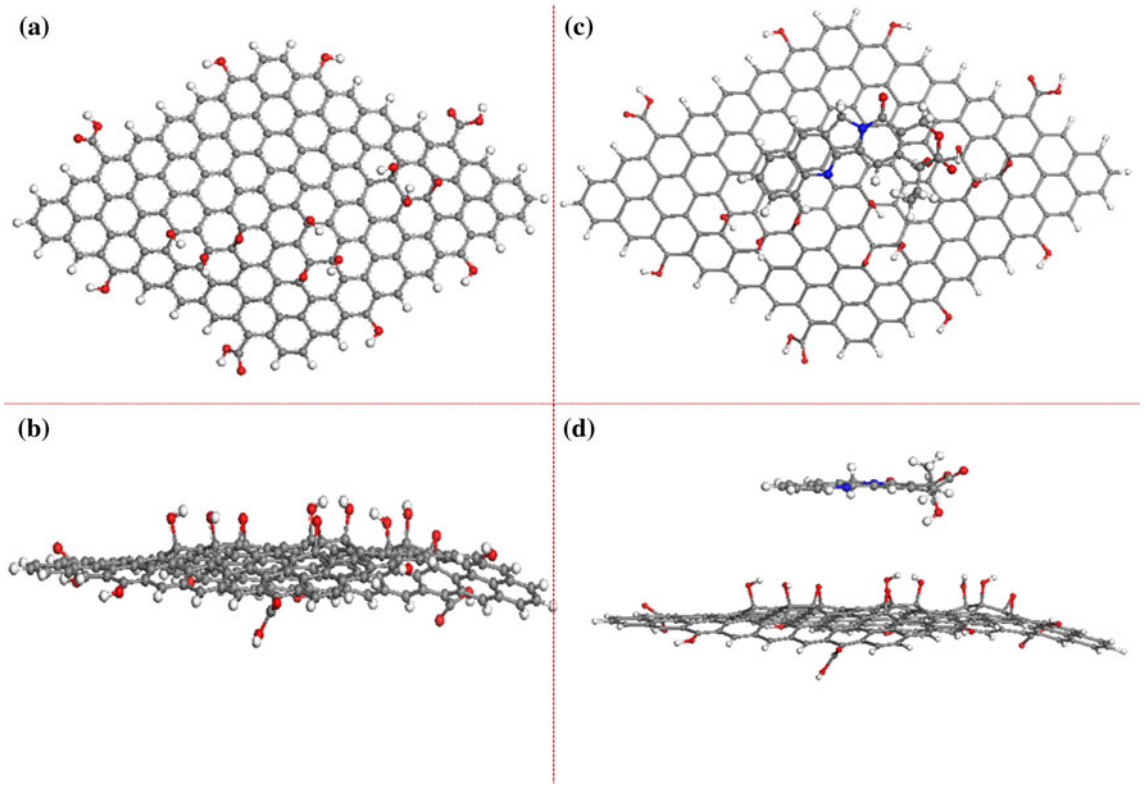

Fig. 5 The optimized geometry depicting **a** front view of 8 × 8 GO sheet, **b** corresponding side view, **c** front view of CPT adsorbed onto 8 × 8 GO sheet, **d** corresponding side view

Fig. S4b, d, and f) whereas LUMO remain delocalized on CPT molecule for CPT/5 × 5 C doped (Supporting Information, Fig. S5b) and CPT/6 × 6 C doped BN nanosheets (Supporting Information, Fig. S5d), respectively whereas for CPT/8 × 8 C doped BN nanosheets the LUMO gets delocalized on the C doped region of the BN sheets with no contribution on adsorbed CPT molecule (Supporting Information, Fig. S5f). For B_xN_y doped graphene sheet (Supporting Information, Fig. S6a, c, e), the HOMO orbital distribution basically represent the edge states having greater charge localization compared to the central BN domain. The LUMO on the other hand has contribution along the edges of the nanosheet rather than the inner basal aromatic rings similar to that of HOMO (Supporting Information, Fig. S7a, c and e). Upon adsorption of CPT, the trend in HOMO (Supporting Information, Fig. S6b, d, and f) and LUMO (Supporting Information, Fig. S7b, d and f) is retained suggesting the contribution to electronic states from the nanosheet rather than adsorbed CPT. Thus, the frontier orbital contribution to HOMO and LUMO shows that except for BN nanosheet/CPT and CPT/C_z doped BN nanosheet systems, in all the other studied nanosheets, the weakly adsorbed CPT does not influence the electronic states of perfect/doped graphene and BN nanosheets.

The frontier orbital contribution towards the HOMO in GO (Supporting Information, Fig. S8a and b) remain localized on the functional groups of GO situated both at the surface and edge states. The LUMO also depicts a similar trend with the contribution from the functional units of GO sheet rather than the aromatic rings of graphene (Supporting Information, Fig. S9a and b). With functionalization of PZA no significant variation in frontier orbital contribution toward the HOMO (Supporting Information, Fig. S8c and d) and LUMO (Supporting Information, Fig. S9c and d) are observed, suggesting the contribution to the electronic states are basically from GO rather than the adsorbed CPT molecule.

Molecular docking

Employing molecular docking we further investigated the preferential binding of CPT drug, graphene functionalized CPT, and CPT functionalized GO with Top1 as discussed below in subsequent subsections.

Docking of bare CPT onto Top1

The 67 K *N*-terminal fragment of Top 1 is a single polypeptide with an extensive secondary structure as observed

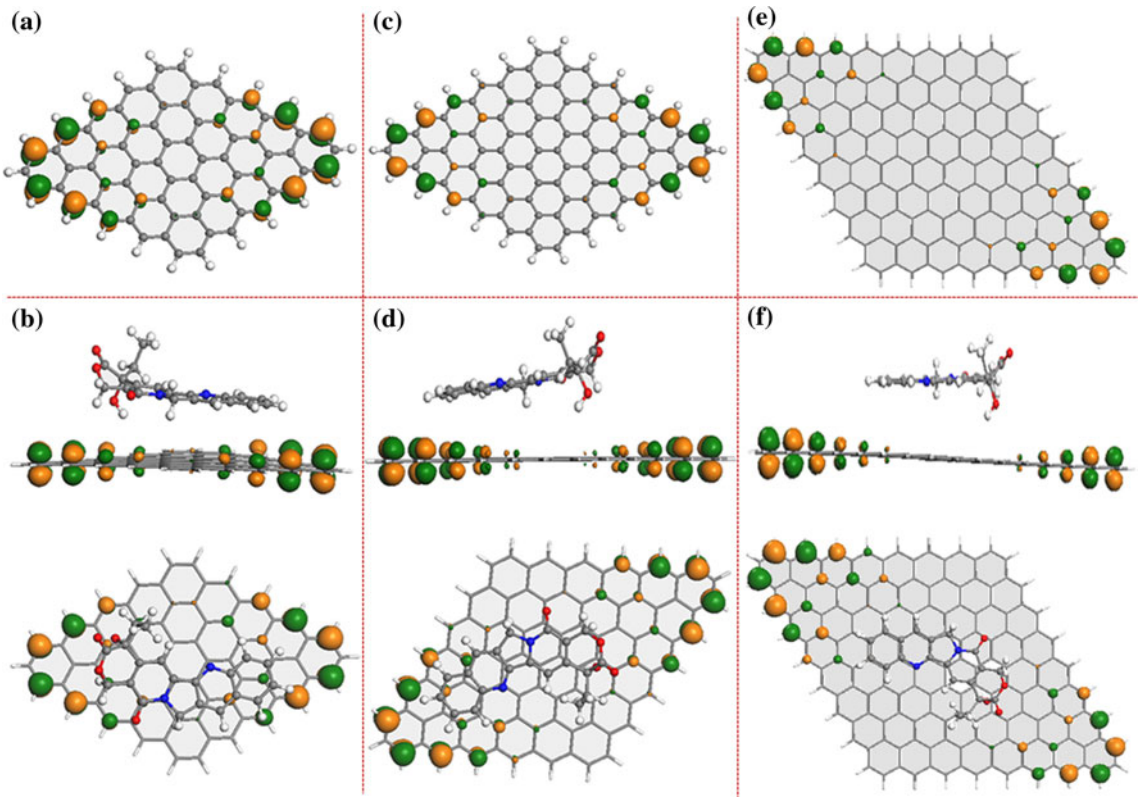

Fig. 6 The HOMO frontier orbital depiction of **a** 5 × 5 graphene, **b** CPT adsorbed onto 5 × 5 graphene sheet depicting the side and front views, **c** 6 × 6 graphene, **d** CPT adsorbed onto 6 × 6 graphene sheet depicting the side and front views, **e** 8 × 8 graphene, **f** CPT adsorbed onto 8 × 8 graphene sheet depicting the side and front views

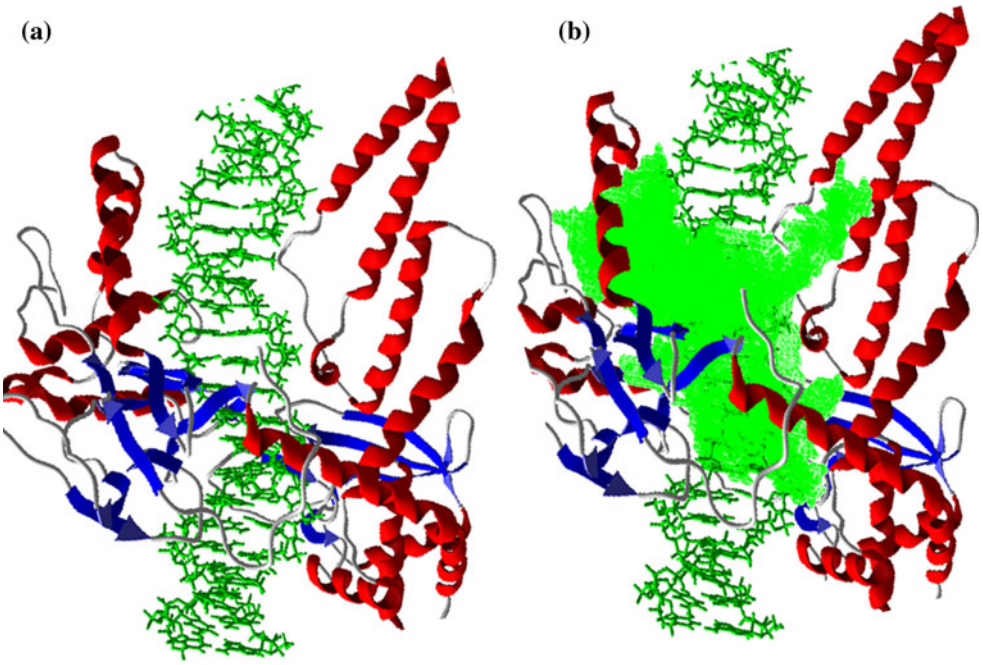

Fig. 7 **a** Secondary structure of DNA Top 1 with the DNA helix shown in green, **b** secondary structure of the protein depicting the binding cavity for CPT drug molecule

from Fig. 7a. There is a 27 Å cavity in the centre of protein large enough to encircle either a single-stranded (ss) or double-stranded (ds) DNA without any steric hindrance between the DNA sugar-phosphate backbone and protein side chains within the torus. The polypeptide cavity is lined with basic residues that provide strong electrostatic

attraction to the negatively charged phosphate oxygen of DNA backbone. Thus, both the size and electrostatic character of the torus make it a likely candidate for temporarily holding a DNA segment. Figure 7b represents the secondary structure of Top1 depicting the binding cavity (shown in green) where the active CPT and nanosheet/CPT systems have be docked to study the interaction and binding with Top 1 protein.

The docking of bare CPT drug onto Top1 (Fig. 8a) shows CPT molecule to be stacked between the Watson–Crick AT and GC base pairs and the interaction is mediated by π–π stacking between the conjugated aromatic ring of CPT and DNA nucleobases (Fig. 8b). The optimum interacting distance of CPT from AT and GC bases are calculated to be 3.874 and 3.377 Å, from the central aromatic rings (Fig. 8b). CPT undergoes strong interaction within DNA nucleobases which probably can play a significant determining role towards drug activity and mode of binding. The electrostatic surface of CPT docked within Top1 (Fig. 10a) shows CPT molecule to lie within the active binding region of protein. The re-rank score of bare CPT drug is calculated to be −89.014 arbitrary unit with a H bond score of −2.529 arbitrary unit as observed in Table 3.

Docking of CPT functionalized graphene with Top1

Likewise, when we compared the docking of CPT supported 8 × 8 graphene with Top1 (Fig. 9) CPT molecule remains docked between the AT and GC base pairs. However, the graphene sheet exhibits a preferential selectivity to strongly bind with ds-DNA helix rather than the protein as observed from Fig. 9b indicating strong interaction between the polar phosphate backbones of the DNA helix. Compared to the docking of bare CPT drug, presence of graphene nanosheet stabilizes the drug molecule as observed from the increase in re-rank score values of CPT molecule (Table 3). The electrostatic surface for CPT functionalized graphene with Top1 demonstrates both CPT and graphene to be grooved within the binding cavity of Top 1 (Fig. 10c, d) undergoing strong interactions with DNA.

Table 3 The re-rank scores and H bond scores for the best docked conformations of bare CPT drug and noncovalent functionalization of CPT onto 8 × 8 graphene, and 8 × 8 GO sheets, respectively

System	Re-rank score CPT	Re-rank score nanosheet	H bond score CPT	H bond score nanosheet
CPT_Top1	−89.014	–	−2.529	–
8 × 8 graphene/CPT docked onto Top1	−89.098	95.867	−2.570	0.000
8 × 8 GO/CPT docked onto Top1	−90.213	126.208	−2.287	−4.437

The parameters are in arbitrary units

Docking of CPT functionalized GO with Top1

The docking of CPT functionalized GO with Top1 as illustrated in Supporting Information, Fig. 10a, depict the CPT molecule to get docked within AT and GC base pairs of DNA. GO undergoes strong interactions with DNA

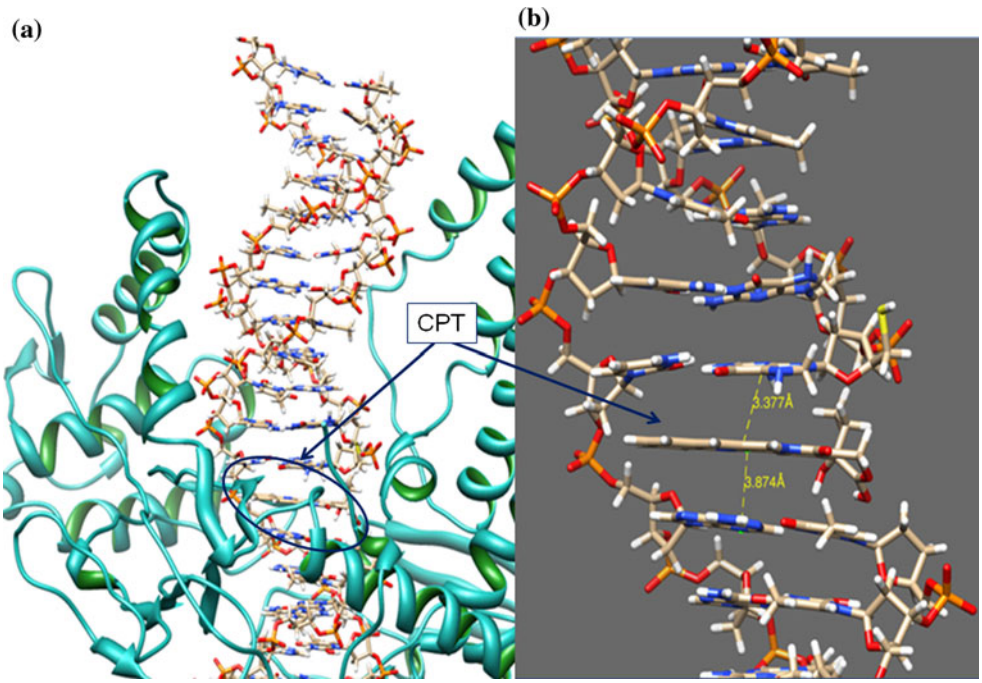

Fig. 8 **a** Secondary structure of Top1 protein with the CPT drug docked within the DNA, **b** optimum interacting distance between docked CPT molecule and the DNA base pairs of Top 1

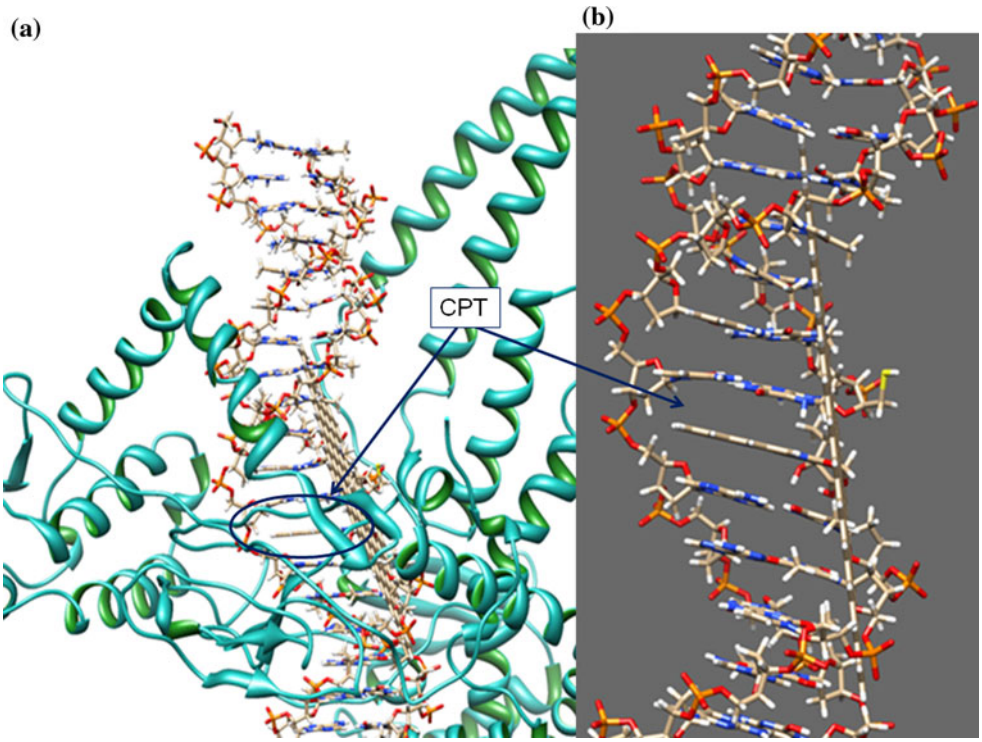

Fig. 9 **a** Secondary structure of Top1 protein with the CPT drug functionalized onto 8 × 8 graphene sheet docked within the DNA, **b** the binding of CPT functionalized 8 × 8 graphene sheet with DNA base pairs of Top 1

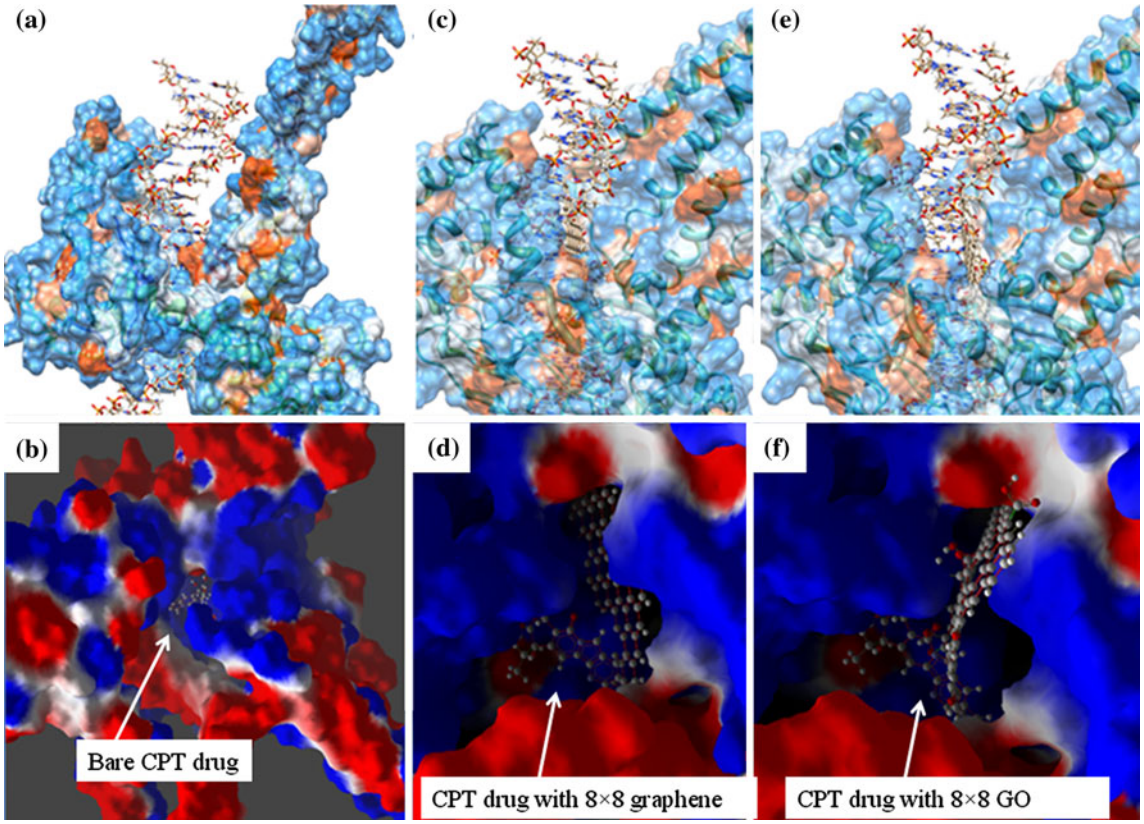

Fig. 10 Secondary structure depicting the hydrophobic surface of **a** bare CPT drug docked within the binding cavity of Top 1, **b** close view showing the interaction within the binding cavity, **c** CPT functionalized 8 × 8 graphene sheet docked within the binding cavity of Top 1, **d** close view showing the interaction within the binding cavity, **e** CPT functionalized 8 × 8 GO sheet docked within the binding cavity of Top 1, **f** close view showing the interaction within the binding cavity

bases and gets docked between the DNA helix and the interaction is basically governed by H-bonded interaction between polar functional units on the basal plane of GO and nucleobases (Supporting Information, Fig. 10b). Compared to graphene sheet, GO exhibits a higher re-rank score value, and H bond score of −4.437 arbitrary unit (Table 3) suggesting the possibility of H-bond with the functional groups of GO and the polar functional groups of the DNA helix. The electrostatic surface for CPT functionalized GO with Top1 demonstrates both CPT and GO to be well docked within the binding cavity of protein (Fig. 10e, f) quite similar to the trend observed for graphene. Thus compared to docking of bare CPT onto Top1 which exhibit comparatively lower re-rank score and H bond score values, presence of graphene and GO support renders significant thermodynamic stability to CPT molecule with higher re-rank and H bond scores values.

Thus we observe that graphene and GO undergoes strong interaction with DNA and Top1 protein and incorporation of graphene and GO nanomaterials for active drug delivery of CPT can lead to significant impetus in the drug delivery regime.

Conclusions

In this work we have demonstrated a comparative study on the structure and energetics towards noncovalent functionalization of CPT anticancer drug with graphene and its prototypes like BN nanosheets, BN doped graphene and C doped BN nanosheets along with GO. The noncovalent functionalization of graphene and related nanomaterials with CPT is mediated by π–π stacking interaction whereas in case of GO it is through the polar functional groups covalently functionalized onto the basal plane of GO. For nanosheets of higher dimension, CPT adsorption results in significant crumpling of the nanosheets due to the high extent of delocalization of aromatic ring present in CPT molecule and graphene surface along with subsequent increase in adsorption energy values within the optimum distance of interaction. The incorporation of BN and C domain segregated within graphene and BN nanosheets result in increase in reactivity (lowering in stability) compared to perfect graphene and BN nanosheets and CPT adsorption onto doped nanosheets yield significantly higher adsorption energy values. Within the limitations of DFT calculations which cannot accurately account for the weak noncovalent interactions inclusion of DFT-D corrections provide better representation towards the adsorption energy values compared to DFT-GGA level of calculations with significant increase in dipole moment of the systems upon functionalization. Frontier orbital analysis help to get a pictorial depiction to the charge delocalization within the nanosystems upon adsorption of CPT molecule. Finally molecular docking studies on bare CPT drug and CPT functionalized onto graphene and GO systems show that the interaction of CPT with Top1 is basically mediated by the π-stacking interaction between the aromatic rings of CPT and the adenine and cytosine bases of DNA helix. However, in presence of CPT supported onto graphene and GO, CPT undergoes a similar trend in adsorption with the DNA nucleobases whereas the graphene and GO support gets docked within the DNA chain suggesting a strong preferential interaction of the nanosheets with DNA. Presence of the nanosheet renders stability to CPT drug molecule as observed from the re-rank and H bond score values. Thus through our study we present a theoretical understanding towards the nature of interaction and energetics for adsorption of CPT onto graphene and related nanomaterials and provides new scopes to broaden up the spectrum of application especially in the field of cancer therapy.

Acknowledgments The authors thank the Department of Science and Technology (DST), New Delhi, India for funding the project.

References

1. Novoselov KS, Geim AK, Morozov SV, Jiang D, Zhang Y, Dubonos SV, Grigorieva IV, Filrsov AA (2004) Electric field effect in atomically thin carbon films. Science 306:666–669
2. Gunlycke D, Lawler HM, White CT (2007) Room-temperature ballistic transport in narrow graphene strips. Phys Rev B 75: 085418-1–085418-5
3. Novoselov KS, Jiang Z, Zhang Y, Morozov SV, Stormer HL, Zeitler U, Maan JC, Boebinger GS, Kim P, Geim AK (2007) Room-temperature quantum hall effect in graphene. Science 315:1379
4. Zhang Y, Tan Y-W, Stormer HL, Kim P (2005) Experimental observation of the quantum hall effect and Berry's phase in graphene. Nature 438:201–204
5. Bolotin KI, Sikes KJ, Jiang Z, Klima M, Fudenberg G, Hone J, Kim P, Stormer HL (2008) Ultrahigh electron mobility in suspended graphene. Solid State Commun 146:351–355
6. Novoselov KS, Geim AK, Morozov SV, Jiang D, Katsnelson MI, Grigorieva IV, Dubonos SV, Firsov AA (2005) Two-dimensional gas of massless Dirac fermions in graphene. Nature 438:197–200
7. Ren T, Li L, Cai X, Dong H, Liu S, Li Y (2012) Engineered polyethylenimine/graphene oxide nanocomposite for nuclear localized gene delivery. Polym Chem 3:2561–2569
8. Feng L, Zhang S, Liu Z (2011) Graphene based gene transfection. Nanoscale 3:1252–1257
9. Peng C, Hu W, Zhou Y, Fan C, Huang Q (2010) Intracellular imaging with a graphene-based fluorescent probe. Small 6:1686–1692
10. Yang K, Zhang S, Zhang G, Sun X, Lee S-T, Liu Z (2010) Graphene in mice: ultrahigh in vivo tumor uptake and efficient photothermal therapy. Nano Lett 10:3318–3323
11. Mohanty N, Berry V (2008) Graphene-based single-bacterium resolution biodevice and DNA transistor: interfacing graphene derivatives with nanoscale and microscale biocomponents. Nano Lett 8:4469–4476

12. Wang Y, Li Z, Wang J, Li J, Lin Y (2011) Graphene and graphene oxide: biofunctionalization and applications in biotechnology. Trends Biotechnol 29:205–212
13. Zhao J-X, Yu Y-Y, Bai Y, Lu B, Wang B-X (2012) Chemical functionalization of BN graphene with the metal-arene group: a theoretical study. J Mater Chem 22:9343–9350
14. Golberg D, Bando Y, Huang Y, Terao T, Mitome M, Tang C, Zhi C (2010) Boron nitride nanotubes and nanosheets. ACS Nano 4:2979–2993
15. Rubio A, Corkill JL, Cohen ML (1994) Theory of graphitic boron nitride nanotubes. Phys Rev B 49:5081–5084
16. Azevedo S, Kaschny JR, de Castilho CMC, de Brito Mota FA (2007) A theoretical investigation of defects in a boron nitride monolayer. Nanotechnol 18:495707
17. Si MS, Xue DS (2007) Magnetic properties of vacancies in a graphitic boron nitride sheet by first–principles pseudopotential calculations. Phys Rev B: Condens Matter Mater Phys 75:193409
18. Zhang Z, Guo W (2011) Controlling the functionalizations of hexagonal boron nitride structures by carrier doping. J Phys Chem Lett 2:2168–2173
19. Wei X, Wang MS, Bando Y, Golberg D (2011) Electron-beam-induced substitutional carbon doping of boron nitride nanosheets, nanoribbons, and nanotubes. ACS Nano 5:2916–2922
20. Li J, Zhou G, Chen Y, Gu B-L, Duan W (2009) Potential room temperature ferromagnetic O/BN and F/BN bilayers. J Am Chem Soc 131:1796–1801
21. Si MS, Li JY, Shi HG, Niu XN, Xue DS (2009) Divacancies in graphitic boron nitride sheets. Europhys Lett 86(46002):1–6
22. Wang Y, Ding Y, Ni J (2010) Fluorination-induced half-metallicity in zigzag boron nitride nanoribbons: first-principles calculations. Phys Rev B: Condens Matter Mater Phys 81: 193407 1–4
23. Zhou J, Wang Q, Sun Y, Jena Q (2010) Electronic and magnetic properties of a BN sheet decorated with hydrogen and fluorine. Phys Rev B: Condens Matter Mater Phys 81(085442):1–7
24. Tang Q, Zhou Z, Chen Z (2011) Molecular charge transfer: a simple and effective route to engineer the band structures of BN nanosheets and nanoribbons. J Phys Chem C 115:18531–18537
25. Kotakoski J, Krasheninnikov AV, Ma Y, Foster AS, Nordlund K, Nieminen RM (2005) B and N ion implantation into carbon nanotubes: insight from atomistic simulations. Phys Rev B 71(205408):1–6
26. Martins TB, Miwa RH, da Silva AJR, Fazzio A (2007) Electronic and transport properties of boron-doped graphene nanoribbons. Phys Rev Lett 98(196803):1–4
27. Ci L, Song L, Jin C, Jariwala D, Wu D, Li Y, Srivastava A, Wang ZF, Storr K, Balicas L, Liu F, Ajayan PM (2010) Atomic layers of hybridized boron nitride and graphene domains. Nat Mater 9:430–435
28. Manna AK, Pati SK (2011) Tunable electronic and magnetic properties in BxNyCz nanohybrids: effect of domain segregation. J Phys Chem C 115:10842–10850
29. Mukhopadhyay S, Scheicher RH, Pandey R, Karna SP (2011) Sensitivity of boron nitride nanotubes toward biomolecules of different polarities. J Phys Chem Lett 2:2442–2447
30. Mukhopadhyay S, Gowtham S, Scheicher RH, Pandey R, Karna SP (2010) Theoretical study of physisorption of nucleobases on boron nitride nanotubes: a new class of hybrid nano-biomaterials. Nanotechnol 21(165703):1–6
31. Gowtham S, Scheicher RH, Pandey R, Karna SP, Ahuja R (2008) First-principles study of physisorption of nucleic acid bases on small-diameter carbon nanotubes. Nanotechnol 19(125701):1–6
32. Gowtham S, Scheicher RH, Ahuja R, Pandey R, Karna SP (2007) Physisorption of nucleobases on graphene: density-functional calculations. Phys Rev B 76:033401–033404
33. Liu Z, Chen K, Davis C, Sherlock S, Cao Q, Chen X, Dai H (2008) Drug delivery with carbon nanotubes for in vivo cancer treatment. Cancer Res 68:6652–6660
34. Liu Z, Robinson JT, Sun X, Dai H (2008) PEGylated nanographene oxide for delivery of water insoluble cancer drugs. J Am Chem Soc 130:10876–10877
35. Wang K, Ruan J, Song H, Zhang J, Wo Y, Guo S, Cui D (2011) Biocompatibility of graphene oxide. Nanoscale Res Lett 6:1–8
36. Zhang X, Yin J, Peng C, Hu W, Zhu Z, Li W, Fan C, Huang Q (2011) Distribution and biocompatibility studies of graphene oxide in mice after intravenous administration. Carbon 49:986–995
37. di Nunzio MR, Cohen B, Douhal A (2011) Structural photodynamics of camptothecin, an anticancer drug in aqueous solutions. J Phys Chem A 115:5094–5104
38. Hsiang Y-H, Hertzberg R, Hecht S, Liu LF (1985) Camptothecin induces proteinlinked DNA breaks via mammalian DNA topoisomerase I. J Biol Chem 260:14873–14878
39. Wall ME, Wani MC, Natschke SM, Nicholas AW (1986) Plant antitumor agents. J Med Chem 29:1553–1555
40. Jena NR, Mishra PC (2007) A theoretical study of some new analogues of the anti-cancer drug camptothecin. J Mol Model 13:267–274
41. Gallo RC, Whang-Peng J, Adamson RH (1971) Studies on the antitumor activity, mechanism of action, and cell cycle effects of camptothecin. J Natl Cancer Inst 46:789–795
42. Ha SW, Kim YJ, Kim W, Lee CS (2009) Antitumor effects of camptothecin combined with conventional anticancer drugs on the cervical and uterine squamous cell carcinoma cell line SiHa. Korean J Physiol Pharmacol 13:115–121
43. Delley B (1990) An all-electron numerical method for solving the local density functional for polyatomic molecules. J Chem Phys 92:508
44. Mulliken RS (1934) Electronic structures of molecules. XI. Electro affinity, molecular orbitals and dipole moments. J Chem Phys 2:782–793
45. Parr RG, von Szentpaly L, Liu S (1999) Electrophilicity index. J Am Chem Soc 121:1922–1924
46. Frisch MJ, Trucks GW, Schlegel HB, Scuseria GE, Robb MA, Cheeseman JR, Scalmani G, Barone V, Mennucci B, Petersson GA, Nakatsuji H, Caricato M, Li X, Hratchian HP, Izmaylov AF, Bloino J, Zheng G, Sonnenberg JL, Hada M, Ehara M, Toyota K, Fukuda R, Hasegawa J, Ishida M, Nakajima T, Honda Y, Kitao O, Nakai H, Vreven T, Montgomery JA, Jr, Peralta JE, Ogliaro F, Bearpark M, Heyd JJ, Brothers E, Kudin KN, Staroverov VN, Kobayashi R, Normand J, Raghavachari K, Rendell A, Iyengar JC, Tomasi SS, Cossi J, Rega M, Millam NJ, Klene M, Knox JE, Cross JB, Bakken V, Adamo C, Jaramillo J, Gomperts, Stratmann RE, Yazyev O, Austin AJ, Cammi RC, Pomelli JW, Ochterski R, Martin RL, Morokuma K, Zakrzewski VG, Voth GA, Salvador P, Dannenberg JJ, Dapprich S, Daniels AD, Farkas O, Foresman JB, Ortiz JV, Cioslowski J, Fox DJ, Gaussian 09, Revision A.1; Gaussian, Inc.: Wallingford CT, 2009
47. Liu L, Zeng Z, Zeng G, Chen M, Zhang Y, Zhang J, Fang X, Jiang M, Lu L (2012) Study on binding modes between cellobiose and b-glucosidases from glycoside hydrolase family 1. Bioorg Med Chem Lett 22:837–843
48. http://molegro.com/mvd-product.php
49. Bursulaya BD, Totrov M, Abagyan R, Brooks CL (2003) Comparative study of several algorithms for flexible ligand docking. J Comput Aided Mol Des 17:755–763
50. Storn R, Price K (1995) Differential evolution: a simple and efficient adaptive scheme for global optimization over continuous spaces; technical report. International Computer Science Institute, Berkley, CA
51. Yang J-M, Chen C-C (2004) GEMDOCK: a generic evolutionary method for molecular docking. Proteins 55:288–304
52. Zhao Y, Wu X, Yang J, Zeng XC (2011) Ab initio theoretical study of non-covalent adsorption of aromatic molecules on boron nitride nanotubes. Phys Chem Chem Phys 13:11766–11772